

# Path-integral representation for a stochastic sandpile

Ronald Dickman<sup>†</sup> and Ronaldo Vidigal

*Departamento de Física, ICEx, Universidade Federal de Minas Gerais,  
30123-970 Belo Horizonte - MG, Brasil*

(October 30, 2018)

## Abstract

We introduce an operator description for a stochastic sandpile model with a conserved particle density, and develop a path-integral representation for its evolution. The resulting (exact) expression for the effective action highlights certain interesting features of the model, for example, that it is nominally massless, and that the dynamics is via cooperative diffusion. Using the path-integral formalism, we construct a diagrammatic perturbation theory, yielding a series expansion for the activity density in powers of the time.

PACS: 05.70.Ln, 02.50.Ga, 05.10.Gg, 05.40.-a

Short title: Path-integral for sandpile

<sup>†</sup>electronic address: dickman@fisica.ufmg.br

## I. INTRODUCTION

Sandpile models were introduced some fifteen years ago as examples of self-organized criticality (SOC), or scale-invariance in the apparent absence of control parameters [1–5]. Subsequently the appearance of such “spontaneous” criticality was shown to result from a control mechanism that forces the system to a critical point marking a phase transition to an absorbing state [6,7]. In fact, sandpiles with the same local dynamics as the original “self-organized” versions, but with strictly conserved particle density,  $p$ , exhibit an absorbing-state phase transition as  $p$  is varied. Thus the particle density is the temperature-like control parameter for these models.

Sandpiles with strictly conserved particle density (so-called *fixed-energy sandpiles* or FES [8]), exhibit absorbing-state phase transitions [9–11], which have attracted much interest of late, in connection with epidemics [12], catalysis [13,14], and the transition to turbulence [15–17]. While continuous phase transitions to an absorbing state fall generically in the universality class of directed percolation (DP) [18,19], numerical evidence indicates that this is not so for sandpiles [20–23]. The non-DP nature of the transition has been attributed to the coupling of the order parameter (the density of active sites), to a second, conserved field (the local particle density), which relaxes diffusively in the presence of activity, and remains frozen in its absence [24]. Independent of the connection with SOC, fixed-energy sandpiles furnish intriguing examples of phase transitions far from equilibrium, incorporating cooperative relaxation in the form of activated diffusion. Until now, all quantitative results for FES have been numerical, based either on simulations [20,24,21,22], or on coherent-anomaly analysis of a series of  $n$ -site cluster approximations [23]. Phenomenological field theories for sandpiles have been proposed [25–27], but their analysis is far from straightforward. It is therefore of great interest to develop theoretical approaches for FES.

This paper is the first of a series analyzing a stochastic sandpile using operator and path-integral methods. In this work we establish the path-integral representation, and use it to develop a time-dependent perturbation theory that yields an expansion for the activity density in powers of time. In subsequent work the series will be extended and analyzed.

Our analysis uses two principal tools. The first is an operator formalism for Markov processes, of the kind developed by Doi [28], and applied to various models exhibiting nonequilibrium phase transitions [29–33]. The second is an exact mapping, due to Peliti, from the Markov process to a path-integral representation [34,35]. This approach is often used to generate an effective action, which may then be analyzed using renormalization group (RG) techniques [36–38]. In the present instance, however, we use the formalism not as the basis for an RG analysis, but to generate a series expansion for the order parameter. The expansion variable is the time; the coefficients are polynomials in the particle density,  $p$ .

The balance of the paper is organized as follows. In Sec. II we define the model and the master equation governing its dynamics using an operator formalism, which is then mapped to the path-integral representation. Sec. III develops the perturbative expansion of the activity density in powers of time. In Sec. IV, we study some general properties of the diagrammatic expansion, allowing us to simplify and extend the analysis. A brief comparison with simulation results is presented in Sec. V. A summary and discussion of our results is given in Sec. VI.

## II. EVOLUTION OPERATOR

We consider Manna's stochastic sandpile in its fixed-energy (particle-conserving) version [21,39,40]. The configuration is specified by the occupation number  $n_i$  at each site; sites with  $n \geq 2$  are said to be *active*, and have a positive rate of *toppling*. When a site topples, it loses exactly two particles ("grains of sand"), which move randomly and independently to nearest-neighbor (NN) sites. In this work, we adopt a toppling rate of  $n(n-1)$  for a site having  $n$  particles. This choice of rate represents a slight departure from the examples studied previously, in which all active sites have the same toppling rate. The present rate leads to a much simpler evolution operator, and, on the other hand, should yield the same scaling properties, since sandpiles, like critical phenomena in general, exhibit a high degree of universality. (Close to the critical point, the density of sites with  $n \geq 3$  particles is quite low, so that in practical terms our choice of rate should not alter quantitative properties greatly. Since studies of *restricted-height* sandpiles [22,24] reveal that they belong to the same universality class as their unrestricted counterparts, there is good reason to expect that a small change in transition rates, that does not modify the symmetry or conservation laws of the model, will have no effect on critical exponents.) Preliminary simulation results [41] indicate that the model studied here exhibits a continuous phase transition at  $p_c = 0.9493$ , in one dimension; the corresponding value for the model with the same toppling rate for all active sites is  $p_c = 0.94885$  [21].

For simplicity we begin the analysis in one dimension; the generalization to  $d$  dimensions is straightforward. We represent the dynamics of this continuous-time Markov process via the master equation, written in the form [34,35]:

$$\frac{d|\Psi\rangle}{dt} = L|\Psi\rangle,$$

where

$$|\Psi\rangle = \sum_{\{n_i\}} p(\{n_i\}, t) |\{n_i\}\rangle$$

is the probability distribution. Here  $p(\{n_i\}, t)$  is the probability of the configuration

with occupation numbers  $\{n_i\}$ , and the state  $|\{n_i\}\rangle$  is a direct product of states  $|n_j\rangle$ , representing exactly  $n_j$  particles at site  $j$ .

The evolution operator  $L$  is written in terms of creation and annihilation operators, defined via the relations:

$$a_i |n_i\rangle = n_i |n_i - 1\rangle$$

and

$$\pi_i |n_i\rangle = |n_i + 1\rangle.$$

The evolution operator for the one-dimensional stochastic sandpile takes the form,

$$L = \sum_i \left[ \frac{1}{4} (\pi_{i-1} + \pi_{i+1})^2 - \pi_i^2 \right] a_i^2. \quad (1)$$

It is readily seen that  $L$  conserves the number of particles.

It is convenient to work in the Fourier representation; on a lattice of  $N$  sites with periodic boundaries, we introduce the discrete Fourier transform:

$$a_k = \sum_j e^{-ijk} a_j, \quad (2)$$

with inverse

$$a_j = \frac{1}{N} \sum_k e^{ijk} a_k, \quad (3)$$

(and similarly for  $\pi_k$ , etc.), where the allowed values for the wave vector are:

$$k = -\pi, -\pi + \frac{2\pi}{N}, \dots, -\frac{2\pi}{N}, 0, \frac{2\pi}{N}, \dots, \pi - \frac{2\pi}{N}. \quad (4)$$

(To avoid heavy notation, we indicate the Fourier transform by the subscript  $k$ ; the subscript  $j$  denotes the corresponding variable on the lattice.) In Fourier representation,

$$L = -N^{-3} \sum_{k_1, k_2, k_3} \omega_{k_1, k_2} \pi_{k_1} \pi_{k_2} a_{k_3} a_{-k_1 - k_2 - k_3}, \quad (5)$$

where  $\omega_{k_1, k_2} = 1 - \cos k_1 \cos k_2$ .

Since  $L$  is in normal form (all operators  $\pi$  to the left of all operators  $a$ ), we can immediately write the evolution kernel, following Peliti's prescription [34,35]:

$$U_t(\{z_k\}, \{\zeta_k\}) = \int \mathcal{D}\hat{\psi} \mathcal{D}\psi \exp \left[ - \int_0^t dt' \left\{ N^{-1} \sum_k \hat{\psi}_k \dot{\psi}_{-k} + N^{-3} \sum_{k_1, k_2, k_3} \omega_{k_1, k_2} \hat{\psi}_{k_1} \hat{\psi}_{k_2} \psi_{k_3} \psi_{-k_1 - k_2 - k_3} \right\} + N^{-1} \sum_k z_k \psi_{-k}(t) \right], \quad (6)$$

with the boundary conditions  $\psi_k(0) = \zeta_k$  and  $\hat{\psi}_k(t) = z_k$ . (The dot denotes a time derivative;  $\{z\}$  stands for the set of parameters  $z_k$  associated with each wave vector, and similarly for  $\{\zeta\}$ .) The functional integrals are over the variables  $\psi_k$  and  $\hat{\psi}_k$ :

$$\int \mathcal{D}\hat{\psi} \mathcal{D}\psi \equiv \prod_k \int \mathcal{D}\hat{\psi}_k \int \mathcal{D}\psi_k \quad (7)$$

[The product is over the first Brillouin zone, Eq.(4).] In the  $d$ -dimensional case, Eq. (6) remains valid if we let

$$\omega_{\mathbf{k}_1, \mathbf{k}_2} = 1 - \lambda_d(\mathbf{k}_1) \lambda_d(\mathbf{k}_2), \quad (8)$$

with

$$\lambda_d(\mathbf{k}) \equiv \frac{1}{d} \sum_{\alpha=1}^d \cos k_\alpha. \quad (9)$$

The wave vectors now range over the first Brillouin zone in  $d$  dimensions.

The kernel is used to evolve the probability generating function,  $\Phi_t(\{z_j\}) \equiv \sum_{\{n_j\}} p(\{n_j\}, t) \prod_j z_j^{n_j}$ , or its Fourier equivalent,  $\Phi_t(\{z_k\}) \equiv \sum_{\{n_k\}} p(\{n_k\}, t) \prod_k z_k^{n_k}$ , via [34],

$$\Phi_t(\{z_k\}) = \prod_k \int \frac{d\zeta_k d\zeta'_k}{2\pi} e^{-i \sum_k \zeta_k \zeta'_{-k}} U_t(\{z_k\}, \{\zeta_k\}) \Phi_0(\{i\zeta'_k\}) \quad (t \geq 0). \quad (10)$$

We consider an initial product-Poisson distribution, with each site having the same mean number of particles,  $p$ , so that,

$$\Phi_0(\{z_j\}) = \exp \left[ p \sum_j (z_j - 1) \right], \quad (11)$$

corresponding to

$$\Phi_0(\{z_k\}) = \exp [Np(z_{k=0} - 1)], \quad (12)$$

in  $k$ -space. Noting that

$$\int \frac{d\zeta d\zeta'}{2\pi} f(\zeta) e^{i\zeta'(p-\zeta)} = f(p) , \quad (13)$$

we see that for a Poisson initial distribution,

$$\Phi_t(\{z\}) = e^{-Np} U_t(\{z\}; \zeta_k = Np\delta_{k,0}) . \quad (14)$$

Thus the generating function at time  $t$  is  $e^{-Np}$  times the r.h.s. of Eq. (6), evaluated with  $\psi_k(0) = Np\delta_{k,0}$ .

The simplest observables of interest are the mean particle number (at site  $j$ ),

$$\langle n_j \rangle = \left. \frac{\partial \Phi_t(\{z_n\})}{\partial z_j} \right|_{z_n=1} , \quad (15)$$

and the mean activity,

$$\langle n_j(n_j - 1) \rangle = \left. \frac{\partial^2 \Phi_t(\{z_n\})}{\partial z_j^2} \right|_{z_n=1} . \quad (16)$$

In  $k$ -space the condition  $z_j = 1$  for all sites  $j$  becomes  $z_k = N\delta_{k,0}$ . Since the system is translation-invariant it is more convenient to study  $\phi \equiv N^{-1} \sum_j \langle n_j \rangle$  and  $\rho \equiv N^{-1} \sum_j \langle n_j(n_j - 1) \rangle$ . (Note that  $\phi = p$  is a constant of the motion, so this quantity serves principally as a check on our analysis.)

Let

$$U_t(\{z\}, \{\zeta\}) = \int \mathcal{D}\hat{\psi} \mathcal{D}\psi \mathcal{G}'[\psi, \hat{\psi}] , \quad (17)$$

where  $\mathcal{G}'$  represents the exponential in Eq.(6), and let

$$\langle \mathcal{A} \rangle \equiv e^{-Np} \int \mathcal{D}\hat{\psi} \mathcal{D}\psi \mathcal{A} \mathcal{G}'[\psi, \hat{\psi}] \Big|_{z_k=N\delta_{k,0}} , \quad (18)$$

where  $\mathcal{A}$  is a function of the fields  $\psi$  and  $\hat{\psi}$ . Evaluating the derivatives in Eqs. (15) and (16), we have

$$\phi = N^{-1} \langle \psi_{k=0} \rangle \quad (19)$$

and

$$\rho = N^{-2} \sum_k \langle \psi_k \psi_{-k} \rangle . \quad (20)$$

It is convenient at this point to perform a change of variables, letting  $\tilde{\psi}_k = \hat{\psi}_k - N\delta_{k,0}$ . As a result,  $\mathcal{G}'$  gains a factor of  $e^{Np}$  [which cancels the prefactor in Eq. (18)], and the boundary term in the argument of the exponential vanishes when we set  $z_k = N\delta_{k,0}$ . Then we have

$$\langle \mathcal{A} \rangle = \int \mathcal{D}\tilde{\psi} \mathcal{D}\psi \mathcal{A} \mathcal{G}[\psi, \tilde{\psi}], \quad (21)$$

where

$$\mathcal{G}[\psi, \tilde{\psi}] \equiv \exp \left[ -N^{-1} \int_0^t dt' \sum_k \tilde{\psi}_k \dot{\psi}_{-k} + \int_0^t dt' \mathcal{L}_I \right], \quad (22)$$

and where the “interaction” is now:

$$\begin{aligned} \mathcal{L}_I = & -N^{-3} \sum_{k_1, k_2, k_3} \omega_{k_1, k_2} \tilde{\psi}_{k_1} \tilde{\psi}_{k_2} \psi_{k_3} \psi_{-k_1 - k_2 - k_3} \\ & - 2N^{-2} \sum_{k_1, k_2} \omega_{k_1, 0} \tilde{\psi}_{k_1} \psi_{k_2} \psi_{-k_1 - k_2}. \end{aligned} \quad (23)$$

Eq. (22) with  $\mathcal{L}_I \equiv 0$  defines  $\mathcal{G}_0$ ; Eq. (21) with  $\mathcal{G}_0$  in place of  $\mathcal{G}$  defines  $\langle \mathcal{A} \rangle_0$ .

The usual procedure at this point would be to take the continuum (small- $k$ ) limit, generating a field theory for the process. While this is not our purpose in the present work, we note some interesting features of the model in this context. The first is that the interaction  $L$  *contributes nothing* to the quadratic part of the action. (This can be seen immediately from Eq.(1):  $L$  is quartic in the fields.) Thus the resulting theory is nominally massless, and has *no evolution at all* in the Gaussian approximation. (Diffusion, in this model, is cooperative, requiring the presence of at least two particles at the same site.) The action, moreover, contains no parameters whatsoever; the relevant parameter  $p$  is “hidden” in the initial probability distribution. A further difference from continuum descriptions of more familiar processes such as DP [18,19] is that the order parameter is given by  $\langle \psi^2 \rangle$  not  $\langle \psi \rangle$ .

In simulations and cluster approximations [20–23], FES clearly show a continuous phase transition between an active and an absorbing state as the parameter  $p$  is varied, in close analogy to more familiar examples, such as directed percolation. Thus at some more reduced level we might expect to find an *effective* field theory of the usual kind, with a nonzero mass, bare diffusion coefficient, and one or more relevant parameters. Such theories have indeed been proposed for sandpile models [26,27]. They include a second field (the particle density) whose evolution is coupled to that of the order parameter. We leave the systematic derivation of such a description, starting from the present exact action, as a topic for future work.

### III. PERTURBATION THEORY

#### A. Free expectations

To evaluate expectations of the form of Eq. (21) we write

$$\langle \mathcal{A} \rangle = \langle \mathcal{A} e^{\int_0^t dt' \mathcal{L}_I} \rangle_0, \quad (24)$$

with the intention of expanding the exponential. Each term in the expansion (corresponding to a diagram, as specified below), can be evaluated once we have determined the free expectations of products of fields,  $\langle \psi_{k_1}(\tau_1) \cdots \psi_{k_m}(\tau_m) \tilde{\psi}_{q_1}(\kappa_1) \cdots \tilde{\psi}_{q_n}(\kappa_n) \rangle_0$ . As usual, this can be reduced to expectations of a single field and of pairs of fields. To begin, consider

$$\langle \psi_k(s) \rangle_0 = \int \mathcal{D}\tilde{\psi} \mathcal{D}\psi \psi_k(s) \exp \left[ -N^{-1} \int_0^t dt' \sum_k \tilde{\psi}_k \dot{\psi}_{-k} \right]. \quad (25)$$

The integrals over  $\tilde{\psi}_k$  force the condition  $\dot{\psi}_k = 0$ , so that  $\psi_k(s) = \psi_k(0) = Np\delta_{k,0}$ . Evidently, the same reasoning implies that free expectation of a product of  $n$  fields  $\psi$  is  $(Np)^n$  if all the wave vectors are zero, and is zero otherwise. (The fact that a single field has a nonzero expectation may appear unusual, but in fact will not cause any inconvenience. It is possible to make a further change of variables to  $\psi'_k = \psi_k - Np\delta_{k,0}$ , at the cost of introducing four new terms in  $\mathcal{L}_i$ .)

To evaluate free expectations involving  $\tilde{\psi}$ , we define an operator  $\mathcal{K}_q(\tau)$  via the property:

$$\mathcal{K}_q(\tau) \mathcal{G}_0 = \tilde{\psi}_k(\tau) \mathcal{G}_0. \quad (26)$$

Integrating by parts in the exponential, we have

$$\begin{aligned} \frac{\delta}{\delta \psi_{-k}(\tau)} \mathcal{G}_0 &= \frac{\delta}{\delta \psi_{-k}(\tau)} \exp \left[ N^{-1} \int_0^t dt' \sum_{k'} \psi_{k'} \partial_{t'} \tilde{\psi}_{-k'} + p \tilde{\psi}_{k=0}(t=0) \right] \\ &= N^{-1} \partial_\tau \tilde{\psi}_k \mathcal{G}_0. \end{aligned} \quad (27)$$

Recalling that  $\tilde{\psi}_k(t)=0$ , we have

$$\mathcal{K}_q(s) = -N \int_s^t d\tau \frac{\delta}{\delta \psi_{-k}(\tau)}. \quad (28)$$

Thus,



$$\langle \tilde{\psi}_k(s) \rangle_0 = -N \int \mathcal{D}\tilde{\psi} \mathcal{D}\psi \int_s^t d\tau \frac{\delta}{\delta \psi_{-k}(\tau)} \mathcal{G}_0 = 0, \quad (29)$$

where the final result is obtained via functional integration by parts. In the same manner we find the basic contraction (free propagator):

$$\langle \psi_{k'}(u) \tilde{\psi}_k(s) \rangle_0 = -N \int \mathcal{D}\tilde{\psi} \mathcal{D}\psi \int_s^t d\tau \psi_{k'}(u) \frac{\delta}{\delta \psi_{-k}(\tau)} \mathcal{G}_0 = N \delta_{k',-k} \Theta(u-s), \quad (30)$$

where  $\Theta$  denotes the step function. As is usual in this formalism,  $\Theta(0) = 0$  [35]. The free expectation of  $n$  fields  $\tilde{\psi}$  and  $n$  fields  $\psi$  is given by the sum of all products of  $n$  pairwise contractions. In case there are  $m > n$  fields  $\psi$  there are additional factors of  $N p \delta_{k_i,0}$  associated with each uncontracted  $\psi$ .

## B. Perturbative expansion

We now have in hand all the ingredients needed to expand expectations of the form of Eq. (24). The first and second terms in  $\mathcal{L}_I$ , Eq. (23), correspond to vertices with four and three lines (a “4-vertex” and a “3-vertex”, respectively). Each  $\tilde{\psi}_k(\tau)$  must be contracted with a  $\psi_{-k}(\tau')$ , where  $\tau' > \tau$ . (The required factors of  $\psi$  may come from other vertices or from  $\mathcal{A}$ .) We adopt a graphical notation in which fields  $\psi$  ( $\tilde{\psi}$ ) are represented by lines entering (leaving) a vertex. All lines are oriented toward the left, the direction of increasing time. Fig. 1 shows the vertices associated with  $\mathcal{L}_I$ , and the nodes that represent  $\phi$  and  $\rho$ . We refer to the latter as “sinks” since they have no outgoing lines. Uncontracted fields  $\psi$  are called “external lines”.

When we expand the exponential in Eq. (24), the  $n$ -th order term carries a factor  $1/n!$ , and there are  $n$  time integrations,  $\int dt_1 \cdots \int dt_n$ , all over the interval  $[0, t]$ . We absorb the factor  $1/n!$  by fixing the time-ordering  $t \geq t_1 \geq t_2 \geq \cdots \geq t_n \geq 0$ . This imposes certain restrictions on diagram topology, since a field  $\tilde{\psi}$  must always be contracted with a  $\psi$  at a later time. Once this ordering is imposed, the integrand has no further time dependence, and the time integrations yield  $t^n/n!$ .

Before formulating general rules, we study a few examples. Consider

$$\rho = N^{-2} \sum_k \langle \psi_k \psi_{-k} e^{\int_0^t dt' \mathcal{L}_I} \rangle_0. \quad (31)$$

The zeroth-order term is simply:

$$N^{-2} \sum_k \langle \psi_k \psi_{-k} \rangle_0 = p^2, \quad (32)$$

i.e., the initial activity for the product-Poisson distribution. At first order we have the diagrams (a) and (b) shown in Fig. 2. For diagram (a) there is a combinatorial

factor of 2, since there are two ways to contract the lines exiting the vertex with the fields in  $\rho$ ; the contribution from this diagram is

$$-2 \int_0^t d\tau N^{-1} p^2 \sum_k \omega_{k,k} = -p^2 t \quad (33)$$

In graph (b) we see that the condition that uncontracted  $\psi$  fields have  $k=0$  forces the line exiting the vertex to have  $k=0$  as well. But there is then a factor of  $\omega_{0,0}=0$  associated with this vertex, so the contribution due to graph (b) vanishes. In general, we can exclude diagrams in which the two lines entering a 3-vertex have momenta that sum to zero.

At order  $t^2$  we have diagrams (c) — (f) shown in Fig. 2; (d) and (f) vanish for the same reason as (b). (From here on we simply ignore such diagrams.) The contribution of graph (c) is readily obtained: there is a combinatorial factor of 4; the time integrations yield  $t^2/2$ ; there is a remaining factor of  $N^{-2}$  times the square of the sum encountered in graph (a). The result is  $p^2 t^2/2$ . In graph (e) there is a combinatorial factor of 8; its contribution is

$$16(t^2/2)p^3 N^{-1} \sum_k [1 - \cos^2 k][1 - \cos k] = 4p^3 t^2 . \quad (34)$$

It is easy to see that our expansion conserves the particle density. With a one-line sink in place of the two-line sink corresponding to  $\rho$ , there will never be enough factors of  $\psi$  to contract with all the  $\tilde{\psi}$  factors, if use only four-line vertices. On the other hand, if we contract the sink with a three-line vertex, there will be a factor of  $\omega_{0,0}=0$ . Thus  $\phi(t) = \phi(0) = p$ .

### C. Diagram rules

In the analysis that follows it will be convenient to employ the Laplace transform; the factor  $t^n/n!$  then becomes  $1/s^{n+1}$ , where  $s$  is the transform variable. Each diagram in the series for  $\tilde{\rho}(s)$  carries a factor of  $N^{L-3n_4-2n_3-2}$ , where  $L$  is the number of lines (including external lines), and  $n_3$  and  $n_4$  are the numbers of 3-vertices and 4-vertices, respectively. There is exactly one factor of  $N^{-1}$  for each free wave vector sum; from here on, we simply associate such a factor with each sum. We can formalize the foregoing discussion into a set of rules for finding the  $n$ -th order contribution to the order parameter  $\tilde{\rho}(s)$ :

1) Draw all connected diagrams with  $n$  vertices, and a two-line sink to the left of all vertices. It is permissible for a line entering a node to be uncontracted (each external line carries a factor  $p$  and must have momentum zero), but each line exiting a vertex ( $j$ ) must be contracted with a vertex ( $i < j$ ) to the left; there is a factor

of  $\delta_{k',-k}$  associated with each internal line. (Here  $k$  is the wave vector of the line exiting vertex  $j$  and  $k'$  the wave vector entering vertex  $i$ .) Given the restriction noted above, that the sum of the momenta entering a 3-vertex cannot be zero, the rightmost vertex of any diagram must be a 4-vertex. We refer to this (and any other) 4-vertex with two external lines as a *source point*.

2) For each graph there is an overall factor of  $1/s$ , and a combinatorial factor counting the number of ways of realizing the contractions. In the series for  $\rho$ , the combinatorial factor is the product of a factor  $C_V$ , associated with the choice of lines at each vertex (for a fixed set of connections between vertices), and a factor  $C_L$  giving the number of choices of, and connections between vertices, consistent with a given diagram. It is easy to show that  $C_V = 2^Q$ , where  $Q = 1 + n_3 + 2n_4 - \ell - f$ , with  $\ell$  the number of simple loops, and  $f$  the number of source points. By a *simple loop* we mean a pair of vertices directly connected by two lines, as in Fig. 2 (a). The connection factor  $C_L$  is unity for diagrams of three or fewer vertices, but can take nontrivial values for  $n \geq 4$ . Examples are discussed below.

3) Each 3-vertex carries a factor of  $-2s^{-1}\omega_{k,0} = -2s^{-1}[1 - \cos k]$ , where  $k$  is the momentum leaving the vertex. Each 4-vertex carries a factor of  $-s^{-1}\omega_{k_1,k_2}$ , where  $k_1$  and  $k_2$  are the momenta of the lines exiting the vertex.

4) After taking into account all of the  $\delta$ -functions associated with propagators, the remaining free wave vectors are summed over the first Brillouin zone, Eq. (4).

We close this subsection with a discussion of the combinatorial factor  $C_L$ . As noted,  $C_L$  represents the number of distinct choices of vertices, and of connections between vertices, consistent with a given diagram topology. Evidently, diagrams with  $n$  vertices arise when we expand the product  $\mathcal{L}_{I,1}, \dots, \mathcal{L}_{I,n}$ ; by “choice of vertices” we mean whether the 3-vertex, or the 4-vertex, associated with each  $\mathcal{L}_{I,i}$  is selected. The  $n$ -th vertex is, as noted, always a 4-vertex. Of course, if the remaining  $n-1$  vertices of a diagram are all of the same kind, then only one choice exists. In most cases, exchanging the positions a 3-vertex and a 4-vertex yields a different diagram, but this is not always so. Consider, for example, diagram (a) shown in Fig. 3. Let us refer to the  $i$ -th vertex in a given diagram (in order of decreasing time) as  $V_i$ , with  $V_0$  denoting the sink. In this diagram  $V_1$  must be a 3-vertex, and  $V_4$  a 4-vertex, but we are free to choose between  $V_2$  and  $V_3$  as the other 3-vertex. Thus this diagram appears *twice* in the expansion of the activity, so that  $C_L = 2$  in this case. (That  $C_L = 2$ , and not more, rests on the fact that, given the choice of vertices, there is only one way of connecting them to yield the desired topology.)

Next we consider the possibility of different connections among a fixed set of vertices. We use  $[i, j]$  to denote a link between  $V_i$  and  $V_j$ . Consider diagrams (b) and (c) of Fig. 3. For diagram (b), the set of connections between vertices is unique:  $[0, 1]$ ,  $[0, 4]$ ,  $[1, 2]$ ,  $[2, 3]$ , and  $[3, 4]$ , so  $C_L = 1$  for this diagram. For diagram (c), by contrast, there are several different sets of connections that yield the same topology. Evidently, the links between  $V_1$  and  $V_0$ , and between  $V_4$  and  $V_3$ , are obligatory. But

this leaves open the question of which vertex the other outgoing line of  $V_4$  links to, and of which vertex is linked to the other line entering the sink. One readily verifies that the following possibilities exist:

i)  $[0, 1], [0, 2], [1, 4], [2, 3], [3, 4]$ ;

ii)  $[0, 1], [0, 2], [1, 3], [2, 4], [3, 4]$ ;

iii)  $[0, 1], [0, 3], [1, 2], [2, 4], [3, 4]$ .

Thus  $C_L=3$  for diagram (c). Consider, finally, diagram (d) of Fig. 3. If  $V_1$  and  $V_2$  are both 3-vertices, there are two possible sets of connections:

i)  $[0, 1], [0, 2], [1, 3]^2, [2, 4], [3, 4]$ ;

ii)  $[0, 1], [0, 2], [2, 3]^2, [1, 4], [3, 4]$ .

In addition, this diagram can be realized (with a unique set of connections), with  $V_1$  and  $V_3$  as the 3-vertices, so that  $C_L=3$  in this case.

#### D. Examples and some general results

There are seven diagrams at third order (Fig. 4). Diagram (a), which continues the series whose first two terms are (a) and (c) of Fig. 2, is readily shown to yield  $-p^2/s^4$ . Applying the rules to diagram (b) in Fig. 4, we find:

$$16(-2)N^{-2}p^3 \frac{1}{s^4} \sum_k [1 - \cos^2 k] \sum_{k'} [1 - \cos^2 k'] [1 - \cos k'] = -\frac{8}{s^4} p^3. \quad (35)$$

The contribution of diagram (c) is identical. For diagram (d) we have

$$16(-4)N^{-1}p^4 \frac{1}{s^4} \sum_k [1 - \cos^2 k] [1 - \cos k]^2 = -\frac{40}{s^4} p^4. \quad (36)$$

Diagram (e) makes the same contribution. Similar analysis yields  $-18p^3/s^4$  for diagram (f) and  $-32p^3/s^4$  for (g). Collecting results, we have

$$\rho = p^2 - p^2 t + \frac{p^2 t^2}{2} (1+8p) - \frac{p^2 t^3}{6} [1 + 66p + 80p^2] + \mathcal{O}(t^4). \quad (37)$$

In evaluating wave vector sums the following observations are helpful. First, note that any wave vector sum  $N^{-1} \sum_k$  can be written as  $(2\pi)^{-1} \int_{-\pi}^{\pi} dk$ . The analysis is facilitated by use of the identity:

$$I_n \equiv \frac{1}{N} \sum_k (1 - \cos^2 k) [1 - \cos k]^n = 4 \cdot 2^n \frac{(2n+1)!!}{(2n+4)!!}. \quad (38)$$

[This can be shown by writing  $I_n$  as an integral, and letting  $u = 1 - \cos k$  so that

$$I_n = \frac{1}{\pi} \int_0^\pi du u^{n+1/2} \sqrt{2-u}.$$

Integrating by parts one readily finds that

$$I_n = 2 \frac{2n+1}{2n+4} I_{n-1},$$

leading to Eq (38), since  $I_0 = 1/2$ . For convenience we note:  $I_1 = 1/2$ ;  $I_2 = 5/8$ ;  $I_3 = 7/8$ ; and  $I_4 = 21/16$ .] Useful identities in the  $d$ -dimensional case are:

$$\sum_{\mathbf{k}} \lambda_d^2(\mathbf{k}) = \frac{1}{2d},$$

$$\sum_{\mathbf{k}} \lambda_d^4(\mathbf{k}) = \frac{3(2d-1)}{8d^3},$$

and

$$\sum_{\mathbf{k}} \lambda_d(\mathbf{k}) \lambda_d(\mathbf{q} - \mathbf{k}) = \frac{1}{2d} \lambda_d(\mathbf{q}).$$

Two general properties of the expansion are readily verified. First, the leading term at each order is  $p^2(-t)^n/n!$ . This set of contributions sums to  $p^2 e^{-t}$ , describing the relaxation of the initial density of active sites. In  $d$  dimensions this becomes  $p^2 \exp[-(2d-1)t/d]$ . The decay rate,  $(2d-1)/d$ , represents twice the probability that the two particles released by a toppling site move to distinct neighbors, the factor of two representing the toppling rate for a site with exactly two particles.

A second observation is that the highest power of  $p$  appearing at order  $t^n$  is  $p^{n+1}$ , coming from diagrams with one source point and  $n-1$  external lines terminating at 3-vertices. The coefficient of this term can be found as follows. Note that the relevant diagrams consist of  $(n-1)$  3-vertices attached to the lines of the simplest graph (Fig. 2a). The number of realizations of such topologies (that is, the sum of the  $C_L$  over all diagrams of this kind), is given by one half the number of distinct sequences of  $r$  symbols  $A$  and  $n-r-1$  symbols  $B$  ( $A$  and  $B$  corresponding to 3-vertices inserted in one or the other line), summed over  $r$  from  $r=0$  to  $n-1$ . (The factor of one half is required because a pair of sequences that merely exchange  $A$ 's and  $B$ 's in fact represent the same diagram.) The number of such realizations is:

$$\frac{1}{2} \sum_{r=0}^{n-1} \binom{n-1}{r} = 2^{n-2}.$$

Each diagram of this kind has a combinatorial factor  $C_V = 2^{n+1}$ , and an additional factor of  $(-1)^n 2^{n-1} I_{n-1}$  coming from the 3-vertices and the wave vector sum. Using our result for  $I_n$ , we find that this contribution is:

$$(-1)^n 2^{4n-1} \frac{(2n-1)!! p^{n+1} t^n}{(2n+2)!! n!},$$

for  $n \geq 2$ . Call the sum of such contributions  $\rho_{max}(t)$ ; it can be evaluated in closed form by noting that

$$\begin{aligned} \rho_{max}(t) &= \frac{p}{4} \frac{1}{2\pi} \int_{-\pi}^{\pi} dk (1 - \cos^2 k) \sum_{n=2}^{\infty} \frac{(-8pt)^n (1 - \cos k)^{n-1}}{n!} \\ &= \frac{p}{4} \left\{ e^{-8pt} [I_0(8pt) + I_1(8pt)] - 1 \right\} + p^2 t, \end{aligned} \quad (39)$$

where  $I_\nu$  denotes the modified Bessel function. The factors of  $e^{-8pt} I_\nu(8pt)$  imply slow relaxation ( $\sim 1/\sqrt{t}$ ) typical of diffusive processes.

#### IV. DIAGRAMMATIC ANALYSIS

As is evident from the foregoing discussion, many diagrams represent simple variations of those appearing at some lower order. The calculation will be simplified if we can identify classes of related diagrams. To begin we enumerate some ways in which diagrams ( $g'$ ) with  $v+1$  vertices can be formed from a  $v$ -vertex diagram  $g$ .

- a) Insert a 3-vertex into any internal line;  $g'$  has one more external line than does  $g$ . An example is the generation of diagram (e), starting from (a) in Fig. 2.
- b) Replace any 4-vertex by a “4-loop”, consisting of a pair of 4-vertices joined by two lines. Diagram (c) (Fig. 2) is generated from (a) by this process.
- c) Replace any 3-vertex  $V$  by a 4-vertex, contracting the new outgoing line with a *new* 3-vertex inserted in an existing internal line. In case the contraction is to a 3-vertex  $V'$  *on the same line* as  $V$ , and there are *no other vertices on this line*, between  $V$  and  $V'$ , we call the resulting structure a “3-loop”. Starting with diagram (e) in Fig. 2, we may generate (f) and (g) (Fig. 4) by this procedure. Diagram (f) has a 3-loop but (g) does not, since in this case  $V'$  does not lie on the same line as  $V$ .
- d) Insert a 4-vertex into an internal line, contracting one of its outgoing lines to an existing external line. (The vertex associated with the latter must lie to the left of

the new 4-vertex.) Graphs (f) and (g) (Fig. 4) are formed from (e) (Fig. 2) by this means.

e) Add a new 4-vertex to  $g$  by joining its outgoing lines to two external lines in  $g$ . Consider again (e) in Fig. 2; if we join two external lines (one of them associated with the 3-vertex) to a new 4-vertex, the result (after some redrawing) is (g) of Fig. 4.

Now consider the inverse of operations a) - c). Given a graph  $g$  with two or more vertices:

a') Remove all 3-vertices bearing an external line.

b') "Collapse" any 4-loop to a single 4-vertex.

c') Collapse any 3-loop to a 3-vertex.

The systematic application of these steps, until no further subtractions are possible, will be called *reduction* of a diagram. Let us define an *articulation point* as a 4-vertex (other than a source point), which, if removed, will leave the diagram disconnected. (Such a vertex has, by necessity, total momentum zero entering it.) In Fig. 2 only graph (c) has an articulation point, while graphs (a), (b) and (c) of Fig. 4 all possess one or more such point.

We may now define an *irreducible* diagram (IRD) as one free of 3-vertices bearing external lines, free of collapsible loops, and having no articulation points. The simplest irreducible diagram is (a) of Fig. 2; we shall refer to it as the one-loop IRD. At each order only a small minority of the diagrams are irreducible. At second order there are *no* IRDs; the only one at third order is (g) in Fig. 4. The IRDs with four vertices are shown in Fig. 5; there are 23 IRDs with five vertices.

In addition to the local modifications (a - e) described above, we can also form new diagrams via *composition*. Given two diagrams  $g$  and  $g'$  we form the *composite diagram*  $gg'$  by:

i) Deleting the two lines entering one of the source points  $r$  of  $g$ ;

ii) Identifying the sink in  $g'$  with  $r$  in  $g$ .

(If  $g$  and  $g'$  are distinct we can also form  $g'g$ .) Graph (b) of Fig. 4 is composed, in this sense, from (a) and (e) of Fig. 2. Composite graphs are reducible by definition (the two components are joined at an articulation point.) When we have removed all 3-vertices with external lines, and collapsed all collapsible loops in a diagram, the result is either an IRD or a composite of such diagrams.

The expansion up to order  $t^v$  may be organized as follows. First we identify all of the IRDs with  $v$  or fewer vertices. For each such IRD, we evaluate its contribution

and that of all diagrams with  $\leq v$  vertices that are directly reducible to it. There remain the composite diagrams. Let  $\tilde{C}_g(s)$  be the contribution to  $\tilde{\rho}(s)$  due to diagram  $g$ . From the definition of the composition process, we see that the contribution of a composite diagram  $gg'$  to the activity is:

$$\tilde{C}_{gg'} = \frac{s}{p^2} \tilde{C}_g \tilde{C}_{g'}. \quad (40)$$

We make use of this relation as follows. For each IRD  $g^*$ , define

$$\tilde{F}_{g^*}(s) = \frac{s}{p^2} \left[ \tilde{C}_{g^*}(s) + \sum_{g' \succ g^*} \tilde{C}_{g'}(s) \right], \quad (41)$$

as  $s/p^2$  times the sum of contributions due to  $g^*$  and all graphs reducible to it (we use  $g' \succ g^*$  to mean “ $g'$  is reducible to  $g^*$ ”). Now define

$$\tilde{F}(s) = \sum_{g^*} \tilde{F}_{g^*}(s), \quad (42)$$

and

$$\tilde{G}(s) = \sum_{g^*} n_{g^*} \tilde{F}_{g^*}(s), \quad (43)$$

where the sum is over all IRDs, and in the second sum  $n_{g^*}$  is the number of source points in  $g^*$ . Each source point serves as a possible attachment site for the preceding element. Then the sum of (i) all irreducible diagrams, (ii) all diagrams reducible to an IRD, and (iii) all linear composite diagrams is

$$\tilde{\rho}_L(s) = \frac{p^2}{s} \frac{\tilde{F}(s)}{1 - \tilde{G}(s)}. \quad (44)$$

Missing from  $\tilde{\rho}_L$  are *branching* composite diagrams. These are composite diagrams in which at least one component has two or more diagrams attached to its source points. Since diagrams with more than one source point have at least four vertices, branching diagrams must have at least six. Thus  $\tilde{\rho}(s) = \tilde{\rho}_L(s)$  to  $\mathcal{O}(s^{-6})$ . Evaluating  $\tilde{F}$  to and  $\tilde{G}$  to this order, we obtain

$$\begin{aligned} \rho &= p^2 - p^2 t + \frac{p^2 t^2}{2} (1 + 8p) - \frac{p^2 t^3}{6} [1 + 66p + 80p^2] \\ &+ \frac{p^2 t^4}{4!} [1 + 442p + 2076p^2 + 896p^3] \\ &- \frac{p^2 t^5}{5!} [1 + 2842p + 35396p^2 + 52240p^3 + 10752p^4] + \mathcal{O}(t^6). \end{aligned} \quad (45)$$



In  $d$  dimensions the result is:

$$\begin{aligned}
\rho = & p^2 - \gamma p^2 t + \frac{p^2 t^2}{2} \gamma (\gamma + 8p) \\
& - \frac{p^2 t^3}{6} \left[ \gamma^3 + \frac{2p}{d^4} (80d^4 - 56d^3 + 12d^2 - 6d + 3) + \frac{16p^2}{d^3} (8d^3 - 6d + 3) \right] \\
& + \frac{p^2 t^4}{4!} \left[ \gamma^4 + \frac{p}{d^5} (1152d^5 - 960d^4 + 336d^3 - 128d^2 + 36d + 6) \right. \\
& \left. + \frac{4p^2}{d^5} (960d^5 - 368d^4 - 112d^3 - 48d^2 + 108d - 21) + \frac{128p^3}{d^3} (8d^2(d+1) - 9(2d-1)) \right] \\
& + \mathcal{O}(t^5), \tag{46}
\end{aligned}$$

where  $\gamma \equiv (2d-1)/d$ .

## V. COMPARISON WITH SIMULATION

Although the series we have derived are too short to yield reliable predictions for the activity  $\rho(t)$  at long times, it is of interest to consider a preliminary comparison with simulation results, as a check on our analysis. We have simulated the one-dimensional model on lattices of  $L=1000$  and  $2000$  sites, with periodic boundaries; initially  $N=pL$  particles are placed randomly on the lattice, generating a product-Poisson distribution of occupation numbers  $n_j$ . We average over  $5 \times 10^5$  independent realizations of the process.

A typical result is shown in Fig. 6, for  $p=1/2$ . Since this is well below the critical value,  $\rho(t) \rightarrow 0$  as  $t \rightarrow \infty$ . (Note that the average is over all realizations, including those that have fallen into the absorbing state.) The simulation result (data points merging to the bold line) decays quite rapidly at first, and then approaches zero more slowly; a systematic study [41] reveals that the approach to  $\rho=0$  is best characterized as a stretched exponential,  $\rho \sim \exp[-at^\beta]$  with  $\beta \simeq 1/2$ .

Two theoretical curves derived using the series, Eq. (45), are shown in Fig. 6. The upper one is generated by transforming the time series to the variable  $y = [1 - e^{-bt}]/b$ , and then constructing the [3,2] Padé approximant to the  $y$ -series. For  $b$  in the range 0.25 to 0.4 we find good agreement at short times; for  $b=0.35$  (shown here) there is excellent agreement for  $t \leq 10$ , but the theoretical prediction attains a constant, nonzero value thereafter.

Since  $\rho(t)$  must decay to zero in this case, it is interesting to study the series for  $d \ln(\rho/p^2)/dt$ . The latter remains negative for large  $t$ , so that the activity itself decays to zero. The lower curve in Fig. 6 is obtained by transforming the derivative-log series to the variable  $z = 1 - (1+bt)^{-1/3}$  (with  $b=2.7$ ), and forming the [2,2] approximant to the  $z$ -series, which is then used to evaluate  $\ln(\rho/p^2)$  via numerical

integration. The activity does indeed decay to zero, but too rapidly. We obtain very similar results using  $b$  in the range of 2 to 3, and using other transformations, for example  $y$  given above, or a modified  $z$  with the exponent  $1/2$  in place of  $1/3$ . After examining various further transformations and analyses, we conclude that the present series is simply too short to yield useful predictions for long times.

It should be noted that the apparent radius of convergence of the original series (estimated from ratios of successive coefficients), is about  $t < 1/4$  for  $p = 1/2$ ; evidently, the transformation and approximant analysis greatly extends the utility of the series. (For  $p = 1$ , the radius of convergence is about  $t < 1/6$ ; the transformed series agrees well with simulations for  $t \geq 2$ .) Thus, despite the divergence between simulation and theory for times greater than about 10, we regard the present comparison, based as it is on a very short series, as confirming the validity of our analysis. Since the approach to the stationary state is neither exponential nor power-law, we anticipate that a fair number of terms will be required to represent it. Once extended series are available, transformations that are consistent with the asymptotic behavior should yield good numerical estimates.

## VI. DISCUSSION

We have derived an exact path-integral representation for the dynamics of a stochastic sandpile model similar to Manna's sandpile, in a version with strictly conserved particle number. (The key differences are: (1) We analyze a continuous-time process, whereas Manna's model is defined in discrete time; and, (2) The toppling rate for a site with  $n$  particles is  $n(n-1)$  rather than uniform, for all sites with  $n \geq 2$ .) We have argued that such minor differences should not affect scaling properties. The path-integral mapping yields an effective action that is nominally massless and parameter-free, the relevant parameter  $p$  (the particle density), appearing in the initial distribution not the evolution operator. This conclusion applies generally to non-dissipative sandpiles.

In contrast to phenomenological field theories of sandpiles [26,27], in which the order parameter density is coupled to a second slowly relaxing variable (the particle density), the exact action derived in the present work involves but a single field,  $\psi$ , whose expectation is the particle density. The order parameter is given by  $\langle \psi^2 \rangle$ . The derivation of a phenomenological description along the lines of Refs. [26] and [27], starting from the exact action, remains an open question.

We develop a diagrammatic perturbation theory, leading to an expansion for the activity density in powers of time, where the coefficients are polynomials in  $p$ . We point out certain general properties of the expansion: its limiting forms for very small, and very large  $p$ , and the slow, diffusion-like nature of the relaxation. The series provides an important check on other theoretical methods, and on simulation results. While it appears to have a limited radius of convergence, experience with

similar series, for the contact process [31] and for random sequential adsorption [42,32], indicates that under suitable transformation of variables and Padé approximant analysis, useful predictions can be obtained. We present some preliminary numerical evidence for this assertion. Thus, if the series can be extended, it should be possible to investigate scaling properties of the sandpile. We intend to pursue such extensions and analyses in the near future.

## REFERENCES

- [1] P. Bak, C. Tang and K. Wiesenfeld, Phys. Rev. Lett. **59**, 381 (1987); Phys. Rev. A **38**, 364 (1988).
- [2] D. Dhar, Physica A **263** (1999) 4, and references therein.
- [3] G. Grinstein, in *Scale Invariance, Interfaces and Nonequilibrium Dynamics*, NATO Advanced Study Institute, Series B: Physics, vol. 344, A. McKane et al., Eds. (Plenum, New York, 1995).
- [4] D. Sornette, A. Johansen, and I. Dornic, J. Phys. I (France) **5**, 325 (1995).
- [5] A. Vespignani and S. Zapperi, Phys. Rev. Lett. **78**, 4793 (1997); Phys. Rev. E **57**, 6345 (1998).
- [6] R. Dickman, M. A. Muñoz, A. Vespignani, and S. Zapperi, Braz. J. Phys. **30**, 27 (2000). e-print: cond-mat/9910454.
- [7] R. Dickman, Physica A **306**, 90 (2002).
- [8] R. Dickman, A. Vespignani and S. Zapperi, Phys. Rev. E **57**, 5095 (1998).
- [9] J. Marro and R. Dickman *Nonequilibrium Phase Transitions in Lattice Models* (Cambridge University Press, Cambridge, 1999).
- [10] H. Hinrichsen, Adv. Phys. **49**, 815 (2000).
- [11] Various articles on absorbing-state phase transitions are collected in Braz. J. Phys. **30**, (2000).
- [12] T. E. Harris, Ann. Prob. **2** (1974) 969.
- [13] R. M. Ziff, E. Gulari, and Y. Barshad, Phys. Rev. Lett. **56** (1986) 2553.
- [14] See Ch. 5 of Ref. [9].
- [15] Y. Pomeau, Physica D **23** (1986) 3.
- [16] H. Chaté and P. Manville, Phys. Rev. Lett. **58**, 112 (1986).
- [17] T. Bohr, M. van Hecke, R. Mikkelsen, and M. Ipsen, Phys. Rev. Lett. **86** (2001) 5482.
- [18] H. K. Janssen, Z. Phys. B **42** (1981) 151.
- [19] P. Grassberger, Z. Phys. B **47** (1982) 365.
- [20] A. Vespignani, R. Dickman, M. A. Muñoz, and S. Zapperi, Phys. Rev. E **62** (2000) 4564.
- [21] R. Dickman, M. Alava, M. A. Muñoz, J. Peltola, A. Vespignani, and S. Zapperi, Phys. Rev. E **64**, 056104 (2001).
- [22] R. Dickman, T. Tomé, and M. J. de Oliveira, Phys. Rev. E, in press; e-print: cond-mat/0203565.
- [23] R. Dickman, e-print: cond-mat/0204608.
- [24] M. Rossi, R. Pastor-Satorras, and A. Vespignani, Phys. Rev. Lett. **85** (2000) 1803.
- [25] M. Paczuski, S. Maslov, and P. Bak, Europhys. Lett. **27**, 97 (1994); **28**, 295 (1994).
- [26] A. Vespignani, R. Dickman, M. A. Muñoz, and Stefano Zapperi, Phys. Rev. Lett. **81**, 5676 (1998).
- [27] M. A. Muñoz, R. Dickman, R. Pastor-Satorras, A. Vespignani, and S. Zapperi, in *Modeling Complex Systems*, Proceedings of the 6th Granada Seminar on

- Computational J. Marro and P. L. Garrido, eds., AIP Conference Proceedings v. 574 (2001); e-print: cond-mat/0011442.
- [28] M. Doi, J. Phys. A **9**, 1465; 1479 (1976).
  - [29] R. Dickman, J. Stat. Phys. **55**, 997 (1989).
  - [30] R. Dickman and I. Jensen, Phys. Rev. Lett. **67**, 2391 (1991).
  - [31] I. Jensen and R. Dickman, J. Stat. Phys. **71**, 89 (1993).
  - [32] R. Dickman, J.-S. Wang, and I. Jensen, J. Chem. Phys. **94**, 8252 (1991); M. J. de Oliveira, T. Tomé, and R. Dickman, Phys. Rev. A **46**, 6294 (1992).
  - [33] J. Zhuo, S. Redner, and H. Park, J. Phys. A **26**, 4197 (1993).
  - [34] L. Peliti, J. Physique **46**, 1469 (1985).
  - [35] R. Dickman and R. R. Vidigal, e-print: cond-mat/0205231.
  - [36] L. Peliti, J. Phys. A **19**, L365 (1986).
  - [37] B. P. Lee, J. Phys. A **27**, 2633 (1994).
  - [38] F. van Wijland, K. Oerding, and H. J. Hilhorst, Physica A **251**, 179 (1998).
  - [39] S. S. Manna, J. Phys. A **24**, L363 (1991).
  - [40] S. S. Manna, J. Stat. Phys. **59**, 509 (1990).
  - [41] R. Dickman, unpublished.
  - [42] A. Baram and D. Kutasov, J. Phys. A **22**, L251 (1989).

## FIGURE CAPTIONS

Fig. 1. Vertices and sinks in  $\mathcal{L}_I$ ,  $\rho$ , and  $\phi$ .

Fig. 2. One- and two-vertex diagrams in the expansion of the order parameter.

Fig. 3. Diagrams analyzed in the discussion in the combinatorial factor  $C_L$ .

Fig. 4. Diagrams with three vertices. Only (g) is irreducible.

Fig. 5. Irreducible diagrams with four vertices.

Fig. 6. Activity in the sandpile with  $p=1/2$ . The points (merging to a bold line) are simulation results; the curves above and below are series-based predictions discussed in the text.

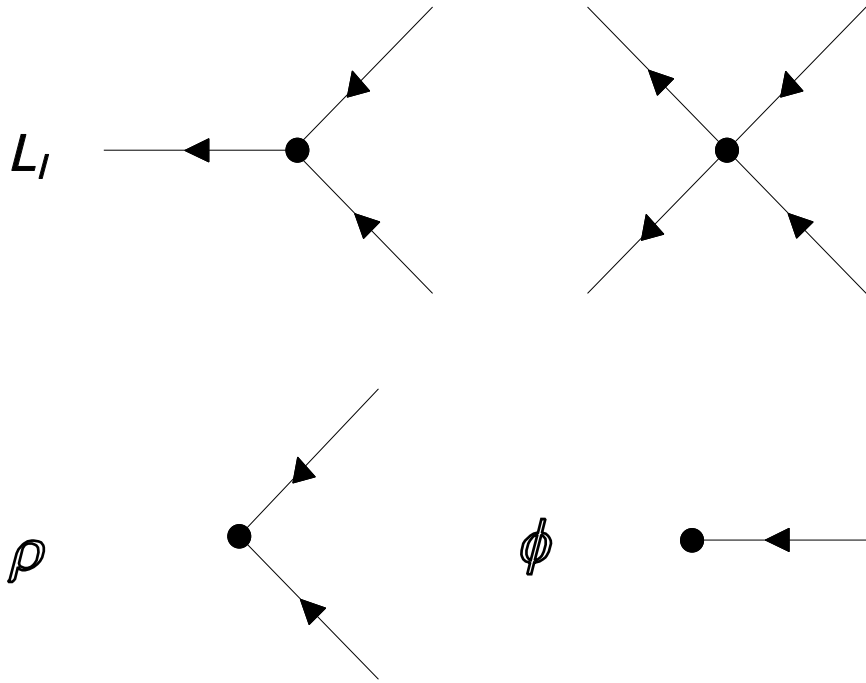


FIG. 1

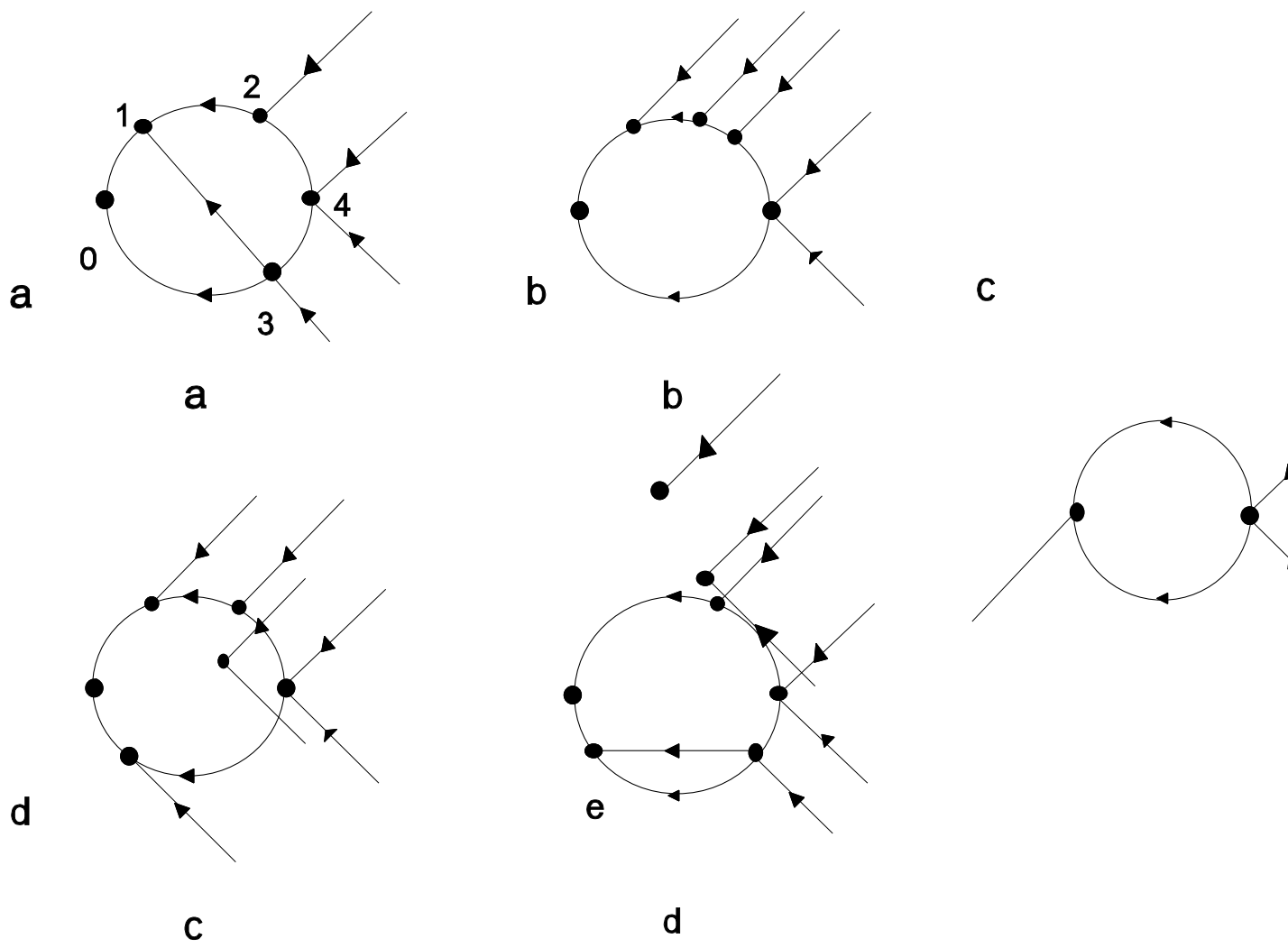
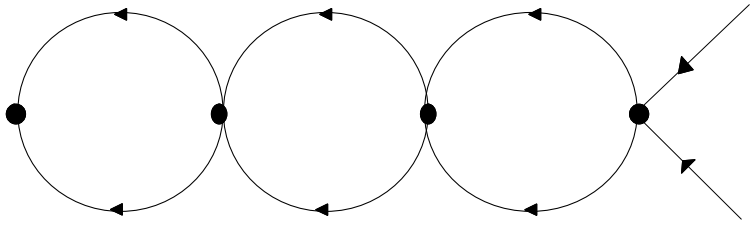
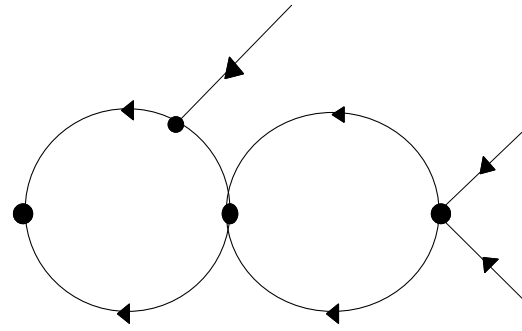


FIG. 3

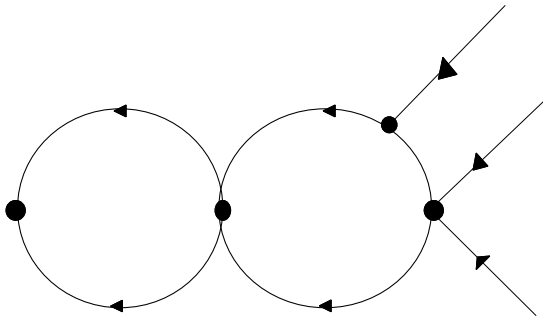




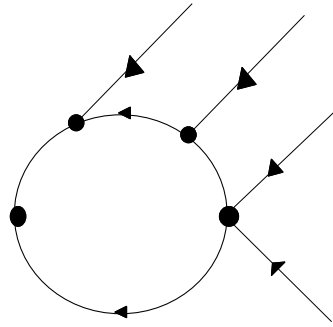
**a**



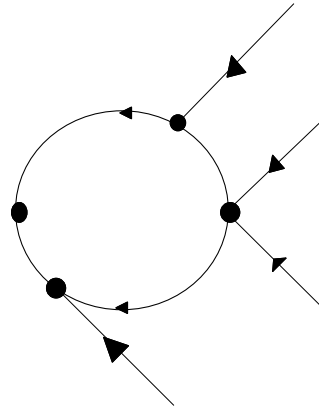
**b**



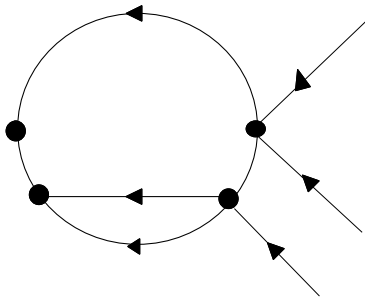
**c**



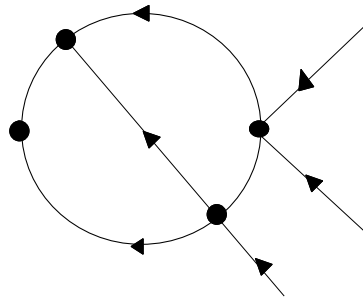
**d**



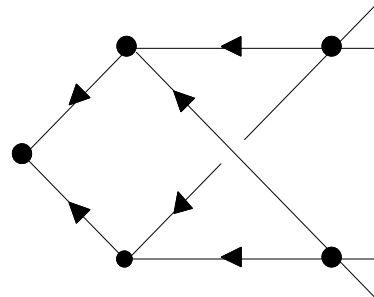
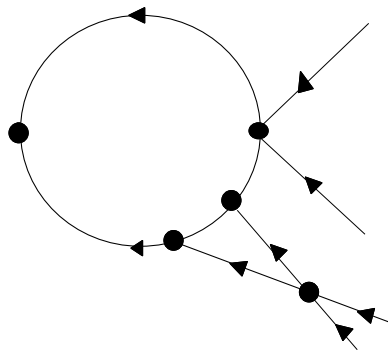
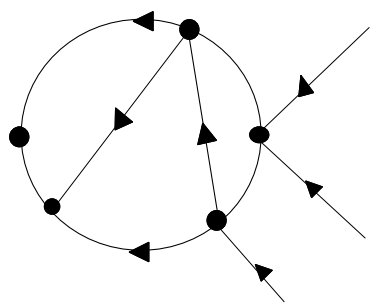
**e**

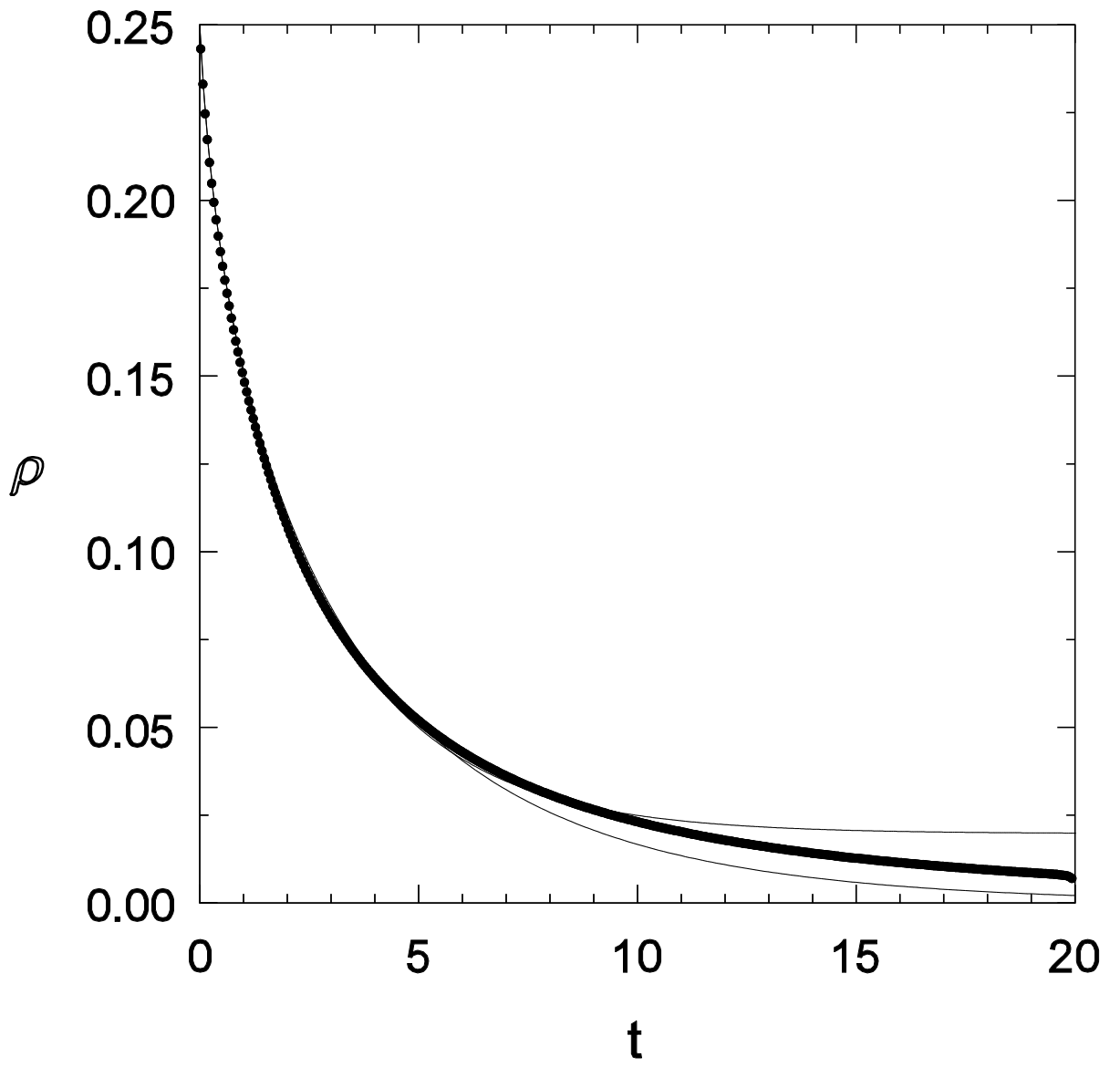


**f**



**g**





FIG